Available online at www.sciencedirect.com
SCIENCE DIRECT®
Journal of Solid State Chemistry 179 (2006) 438–449
JOURNAL OF SOLID STATE CHEMISTRY
www.elsevier.com/locate/jssc

Design and synthesis of four coordination polymers generated from 2,2′-biquinoline-4,4′-dicarboxylate and aromatic bidentate ligands

Junwei Ye, Ping Zhang**, Kaiqi Ye, Hongyu Zhang, Shimei Jiang, Ling Ye, Guangdi Yang, Yue Wang*

Key Laboratory for Supramolecular Structure and Materials of Ministry of Education, College of Chemistry, Jilin University, Changchun 130012, PR China

Received 25 September 2005; received in revised form 3 November 2005; accepted 3 November 2005
Available online 7 December 2005

Abstract

Four coordination polymers $[Zn(bqdc)(phen)]_n$ (**1**), $[Zn(bqdc)(bpy)(H_2O)]_n$ (**2**), $[Mn(bqdc)(bpy)(H_2O)_2]_n$ (**3**) and $[Mn(bqdc)(phen)(H_2O)_2]_n$ (**4**) (H_2bqdc = 2,2′-biquinoline-4,4′-dicarboxylic acid, phen = 1,10-phenanthroline and bpy = 2,2′-bipyridyl) have been synthesized under hydrothermal conditions and characterized by single-crystal X-ray diffraction. Crystal data for **1**: monoclinic system, $C2/c$, $a = 14.141(3)$ Å, $b = 10.021(2)$ Å, $c = 18.511(4)$ Å, $\beta = 103.78(3)^\circ$, $V = 2547.6(9)$ Å^3, $Z = 4$. Crystal data for **2**: monoclinic system, $p2_1/n$, $a = 13.656(3)$ Å, $b = 10.015(2)$ Å, $c = 19.127(4)$ Å, $\beta = 107.13(7)^\circ$, $V = 2500.1(9)$ Å^3, $Z = 4$. Crystal data for **3**: monoclinic system, $C2/c$, $a = 14.5050(8)$ Å, $b = 15.1932(8)$ Å, $c = 12.7549(6)$ Å, $\beta = 116.8010(11)^\circ$, $V = 2508.9(2)$ Å^3, $Z = 4$. Crystal data for **4**: monoclinic system, $C2/c$, $a = 14.1732(17)$ Å, $b = 16.115(3)$ Å, $c = 12.809(3)$ Å, $\beta = 117.04(3)^\circ$, $V = 2605.7(8)$ Å^3, $Z = 4$. Single helix-like chains exist in **1**. The supramolecular structure of **1** exhibits extended two-dimensional network while **2–4** display extended three-dimensional architectures based on interchain hydrogen bonding and $\pi-\pi$ interactions. Compounds **1** and **2** show blue photoluminescence under UV light suggesting that they may be employed to develop luminescent materials. Compounds **3** and **4** show interesting magnetic behaviors.

Keywords: Coordination polymers; Zinc; Manganese; Photoluminescence; Magnetism

1. Introduction

The rational design and self-assembled construction of novel functional metal-organic frameworks (MOFs) has drawn considerable attention in recent years [1–6]. This is due to their intriguing network topologies and diverse potential for scientific and technological applications as molecular separation, selective catalyst, and functional devices [7–12]. Molecular self-assembly has been proven to be an efficient way to obtain extended coordination polymers. In order to construct coordination polymers with novel architectures and properties, covalent bonds and non-covalent interactions, such as hydrogen bonding and $\pi-\pi$ stacking interactions, often were employed simultaneously [13–18]. It is well known that the selection of appropriate organic ligands is crucial to design and synthesize the target coordination polymers [19–21]. In addition, controlling the factors involved in molecular self-assembly process, such as the solvent system, temperature, pH value, are also important [22,23]. The commonly employed strategy for the synthesis of coordination polymers is the self-assembly of metal ion with appropriate linear rigid bridging ligand. We believe that the application of bridging ligands with conformation freedoms is beneficial to the adjustment of structures and the construction of frameworks with novel structures and properties, although the structural control of the product is difficult.

In an effort to obtain coordination polymers with new structures, we utilized a pyridyl-polycarboxylate type ligand 2,2′-biquinoline-4,4′-dicarboxylic acid (H_2bqdc) together with bidentate ligands, 1,10-phenanthroline (phen) and 2,2′-bipyridyl (bpy), to generate coordination polymers. For bqdc bridging ligand, two quinolines are linked together by a single bond and can rotate to each

**Also to be corresponded.
*Corresponding author. Fax: +86 431 5193421.
E-mail address: yuewang@jlu.edu.cn (Y. Wang).

0022-4596/$ - see front matter © 2005 Elsevier Inc. All rights reserved.
doi:10.1016/j.jssc.2005.11.003

other suggesting that bqdc may offer more possibilities geometry configuration and coordination modes towards the metal ions. The bending of the biphenyl group is a crucial parameter for their using and design of appropriate technology. Furthermore, the quinoline derivatives are promising for non-linear optical properties as recently were shown in the literatures [24,25]. The quinoline containing coordination polymer may display some novel optical properties. In this paper, we present the syntheses and single-crystal structures of four coordination polymers, $[Zn(bqdc)(phen)]_n$ **1**, $[Zn(bqdc)(bpy)(H_2O)]_n$ **2**, $[Mn(bqdc)(bpy)(H_2O)_2]_n$ **3**, and $[Mn(bqdc)(phen)(H_2O)_2]_n$ **4**. In **1**–**4**, one-dimensional coordination molecular chains exist. Single helix-like chains were found in **1** and hydrogen bonding and $\pi-\pi$ interactions between one-dimensional chains led to the formation of two-dimensional network. The supramolecular structures of **2–4** display extended three-dimensional architectures based on interchain hydrogen bond. Interchain $\pi-\pi$ interactions were found in **2** and **3**. Compounds **1** and **2** show blue photoluminescence under UV light suggesting that they may be employed to develop luminescent materials. Compounds **3** and **4** show interesting magnetic behaviors.

2. Experimental

2.1. Materials and methods

All reagents, 2,2′-biquinoline-4,4′-dicarboxylic acid (H_2bqdc) (Fluka), 1,10-phenanthroline (phen) (Acros) and 2,2′-bipyridine (bpy) (Acros) were reagent grade and used without further purification. Elemental analysis was performed on a Perkin-Elmer 2400 CHN Elemental Analyzer. Inductively coupled plasma (ICP) analysis was performed on a Perkin-Elmer Optima 3300DV ICP instrument. Thermogravimetric analysis (TGA) was performed on a Perkin-Elmer TGA 7 unit with a heating rate of 10 °C min^{-1}. Absorption spectra were obtained using a PE UV-VIS Lambda 20 spectrometer. Photoluminescence spectra were measured on a Shimadzu RF-5301PC spectrophotometer. FT-IR spectra were recorded on a Bruker IFS 66 V interferometer. Magnetic susceptibility data were collected over the temperature range 2–300 K at a magnetic field of 5 kOe on a Quantum Design MPMS-7 SQUID magnetometer.

2.2. Synthesis and characterization

2.2.1. Synthesis of $[Zn(bqdc)(phen)]_n$ (1)

A mixture of $Zn(CH_3COO)_2 \cdot 2H_2O$ (0.022 g, 0.1 mmol), H_2bqdc(0.034 g, 0.1 mmol), phen (0.020 g, 0.1 mmol), and distilled water H_2O (8 mL) was stirred for 30 min and heated at 453 K for 72 h in a Teflon-lined stainless steel autoclave (25 mL) under autogenously pressure. After cooling to room temperature, the colorless block-shaped crystals were obtained and washed with water and dried in air. The yield was 62% based on Zn. Element analysis calcd (%) for $C_{32}H_{18}N_4O_4Zn$ (587.87): C 65.38%; H 3.09%; N 9.53%; found: C 65.49%; H 3.41%; N 9.63%. IR (KBr, cm^{-1}) data: 1565(s), 1539(m), 1423(s), 1378(vs), 1198(m), 1146(w), 1022(w), 856(m), 807(m), 776(vs), 669(w), 542(w).

2.2.2. Synthesis of $[Zn(bqdc)(bpy)(H_2O)]_n$ (2)

A mixture of $Zn(CH_3COO)_2 \cdot 2H_2O$ (0.044 g, 0.2 mmol), H_2bqdc (0.064 g, 0.2 mmol), bpy (0.064 g, 0.4 mmol) and H_2O (10 mL) was sealed in a Teflon-lined stainless steel autoclave (25 mL) and heated at 413 K for 72 h under autogenously pressure. After cooling to room temperature, yellow block-shaped crystals were collected by filtration and dried in air. The yield was 67% based on Zn. Element analysis calcd (%) for $C_{30}H_{20}N_4O_5Zn$ (581.87): C 61.92%; H 3.46%; N 9.64%; Found: C 61.86%; H 3.41%; N 9.71%. IR (KBr, cm^{-1}) data: 1608(s), 1589(s), 1542(m), 1441(s), 1380(vs), 1202(w), 1151(w), 1024(w), 807(m), 765(vs), 664(w), 540(w).

2.2.3. Synthesis of $[Mn(bqdc)(bpy)(H_2O)_2]_n$ (3)

A mixture of $Mn(CH_3COO)_2 \cdot 4H_2O$ (0.05 g, 0.2 mmol), H_2bqdc (0.034 g, 0.1 mmol), bpy (0.064 g, 0.4 mmol) and H_2O (10 mL) was stirred for 40 min and heated at 453 K for 72 h in a Teflon-lined stainless steel autoclave (25 mL) under autogenously pressure. After cooling to room temperature, yellow large block-shaped crystals were collected by filtration and dried in air. The yield was 69% based on Mn. Element analysis calcd (%) for $C_{30}H_{22}N_4O_6Mn$ (589.46): C 61.13%; H 3.76%; N 9.51%; Found: C 61.09%; H 3.71%; N 9.58%. IR (KBr, cm^{-1}) data: 1565(s), 1539(m), 1444(m), 1380(vs), 1153(w), 1078(w), 893(s), 746(s), 747(s), 656(s), 542(w).

2.2.4. Synthesis of $[Mn(bqdc)(phen)(H_2O)_2]_n$ (4)

A mixture of $MnSO_4 \cdot H_2O$ (0.068 g, 0.4 mmol), H_2bqdc (0.034 g, 0.1 mmol), phen (0.08 g, 0.4 mmol) and H_2O (10 mL) was sealed in a Teflon-lined stainless steel autoclave (25 mL) and heated at 453 K for 96 h under autogenously pressure. After cooling to room temperature, yellow block-shaped crystals were collected by filtration and dried in air. The yield was 60% based on Mn. Element analysis calcd (%) for $C_{32}H_{22}N_4O_6Mn$ (613.49): C 62.65%; H 3.61%; N 9.13%; Found: C 62.61%; H 3.60%; N 9.21%. IR (KBr, cm^{-1}) data: 1561(s), 1517(m), 1423(m), 1383(vs), 1144(w), 1076(w), 891(m), 837(s), 746(vs), 657(s), 535(s).

2.3. X-ray crystallography

The crystal structures were determined by single-crystal X-ray diffraction experiment. The reflection data were collected on a Rigaku R-AXIS RAPID diffractometer (Mo$K\alpha$ radiation, graphite monochromator) at room temperature with ω-scan mode. Empirical absorption correction was applied foe all data. The structure was solved by direct methods and refined by full-matrix least

Table 1
Crystallographic data for **1–4**

	1	**2**	**3**	**4**
Empirical formula	C_{32} H_{18} N_4 O_4 Zn	C_{30} H_{20} N_4 O_5 Zn	C_{30} H_{22} Mn N_4 O_6	C_{32} H_{22} Mn N_4 O_6
Formula weight	587.87	581.87	589.46	613.48
Wave length (Å)	0.71073	0.71073	0.71073	0.71073
Crystal system	Monoclinic	Monoclinic	Monoclinic	Monoclinic
Space group	*C*2/*c*	*P*2(1)/*n*	*C*2/*c*	*C*2/*c*
a (Å)	14.141(3)	13.656(3)	14.5050(8)	14.1732(17)
b (Å)	10.021(2)	10.015(2)	15.1932(8)	16.115(3)
c (Å)	18.511(4)	19.127(4)	12.7549(6)	12.809(3)
β (deg)	103.78(3)	107.13(3)	116.8010(11)	117.039(2)
Volume (Å^3)	2547.6(9)	2500.1(9)	2508.9(2)	2605.7(8)
Z	4	4	4	4
$D_{CalcD.}$ (mg/m^3)	1.533	1.546	1.561	1.564
F_{000}	1200	1192	1212	1260
Crystal size (mm)	0.51 × 0.20 × 0.16	0.41 × 0.35 × 0.35	0.52 × 0.35 × 0.14	0.57 × 0.24 × 0.10
Theta range for data collection (deg)	2.27/27.27	3.02/ 27.47	2.07/27.48	2.05/27.48
Limiting indices	$0\leqslant h\leqslant 18$, $0\leqslant k\leqslant 12$, $-23\leqslant l\leqslant 23$	$-17\leqslant h\leqslant 17$, $-12\leqslant k\leqslant 12$, $-24\leqslant l\leqslant 21$	$0\leqslant h\leqslant 18$, $0\leqslant k\leqslant 19$, $-16\leqslant l\leqslant 14$	$0\leqslant h\leqslant 18$, $0\leqslant k\leqslant 20$, $-16\leqslant l\leqslant 14$
R (int)	0.024409	0.0192	0.028477	0.028994
Data/restraints/parameters	2558/0/222	5627/0/369	2884/0/231	2989/0/239
Goodness-of-fit on F^2	1.077	1.096	0.931	0.955
R_1 $[I>2\sigma(I)]$[a]	0.0333	0.0289	0.0287	0.0313
wR_2 $[I>2\sigma(I)]$[a]	0.0923	0.0811	0.0731	0.0745
R_1 (all data)[a]	0.0434	0.0346	0.0418	0.0504
wR_2 (all data)[a]	0.0948	0.0832	0.0771	0.0829
Residuals (e/Å^3)	0.303/−0.287	0.285/−0.331	0.362/−0.393	0.342/−0.515

[a] $R_1 = \Sigma\|F_o|-|F_c\|/\Sigma|F_o|$; $wR_2 = \{\Sigma[w(F_o^2-F_c^2)^2]/\Sigma[w(F_o^2)]^2\}^{1/2}$.

squares on F^2 using SHELXTL97 software [26]. Empirical adsorption correction was applied for all date. The heaviest atoms were firstly located. O and C atoms were subsequently located in difference Fourier maps. All non-hydrogen atoms were refined anisotropically. The hydrogen atoms of **1**, **3** and **4** were located in difference Fourier maps. The positions of hydrogen atoms of **2** were calculated by geometric models. Experimental details for the structure analysis are given in Table 1, selected bond distances and angles in Table 2, the hydrogen bonds in Table 3, respectively.

3. Results and discussion

3.1. Synthesis

Compounds **1–4** were synthesized from H_2bqdc and Zn(II) or Mn(II) in the presence of phen or bpy under hydrothermal condition. Preliminary studies demonstrated that the reaction temperature was crucial to the products. For the synthesis of **1** and **4**, the reaction temperature must be controlled at 453 K. If the temperature was below 453 K, we can not obtain **1** or **4**. In contrast, **2** and **3** were prepared with good yields when the reaction temperature varied from 413 to 453 K. The synthesis of **1** with Zn(II), H_2bqdc and phen in the ratio of 1:1:1 gave high quality crystals of **1** with good yield. To obtain high quality crystals of **2,** excess of bpy was needed and the ratio between Zn(II), H_2bqdc and bpy was 1:1:2. We also found that excess of Mn(II) and bpy or phen were necessary for the synthesis of **3** and **4**. The mixture of Mn(II), H_2bqdc and bpy in a 2:1:4 ratio leaded to the formation of crystals of **3** with relatively high yield. The reaction mixture of Mn(II), H_2bqdc and phen in a 4:1:4 ratio afford good quality crystals of **4** with high yield. Although **2**, **3** or **4** could be obtained when the ratio of metal, H_2bqdc and phen (or bpy) was 1:1:1, the crystals quality was poor.

3.2. IR, thermal characterizations and stability

The FT-Infrared (IR) spectrum of **1** exhibits antisymmetric carboxylate stretching band and C═C (or N═N) stretching vibrations in the region of 1530–1620 cm^{-1}. The bands in region of 1370–1440 cm^{-1} in IR spectrum are likely due to the symmetric carboxylate stretching band and C═C stretching vibrations. We suggest that the IR bands in the region of 650–880 cm^{-1} can be assigned to the CH in plane and out-of-plane bending modes. The IR spectra of **2–4** display similar characteristic to **1**.

The thermal behaviors of **1–4** were examined by TGA under atmosphere. The TGA result indicates that **1** does not decomposition up to 406 °C. The total weight loss of 85.92% between 406 and 603 °C is consistent with the weight loss of bqdc and phen ligands. The remaining

Table 2
Bond lengths (Å) and angles (deg) for **1–4**

1			
Zn–O(1)	2.2255(18)	Zn–O(1)#1	2.2255(18)
Zn–O(2)	2.1027(16)	Zn–O(2)#1	2.1027(16)
Zn–N(2)	2.097(2)	Zn–N(2)#1	2.097(2)
O(1)–Zn–O(1) $^{\#1}$	98.45(10)	O(2)–Zn–O(1)	90.29(7)
O(2)–Zn–O(1)	60.59(7)	O(2)–Zn–O(2)#1	136.32(10)
O(2) $^{\#1}$–Zn–O(1)	90.29(7)	O(2)#1–Zn–O(1)#1	60.59(7)
N(2)–Zn–O(1)	92.03(8)	N(2)#1–Zn–O(1)#1	92.03(8)
N(2)–Zn–O(1) $^{\#1}$	165.73(7)	N(2)#1–Zn–O(2)#1	103.34(7)
N(2)–Zn–O(2)	103.34(7)	N(2)#1–Zn–O(1)	165.73(7)
N(2)–Zn–O(2) $^{\#1}$	109.97(7)	N(2)#1–Zn–O(2)	109.97(7)
N(2) $^{\#1}$–Zn–N(2)	79.46(12)		
2			
Zn–O(1)	1.9735(15)	Zn–O(3)$^{\#1}$	2.3870(17)
Zn–O(4)$^{\#1}$	2.1103(15)	Zn–O(5)	2.1068(15)
Zn–N(3)	2.1044(16)	Zn–N(4)	2.1651(17)
O(1)–Zn–O(4)$^{\#1}$	171.72(6)	O(1)–Zn–N(3)	95.27(7)
O(1)–Zn–O(5)	90.86(6)	O(1)–Zn–N(4)	95.96(6)
O(1)–Zn–O(3)$^{\#1}$	114.05(6)	O(4)$^{\#1}$–Zn–N(4)	85.67(6)
O(4)$^{\#1}$–Zn–O(3)$^{\#1}$	57.80(6)	N(3)–Zn–O(3)$^{\#1}$	148.72(6)
O(5)–Zn–O(3)$^{\#1}$	92.84(6)	N(3)–Zn–O(4)$^{\#1}$	93.00(7)
O(5)–Zn–O(4)$^{\#1}$	88.25(6)	N(3)–Zn–O(5)	97.55(6)
O(5)–Zn–N(4)	171.69(6)	N(3)–Zn–N(4)	77.15(6)
3			
Mn–O(1)	2.1494(11)	Mn–O(1)$^{\#1}$	2.1494(11)
Mn–O(3)	2.2339(11)	Mn–O(3)$^{\#1}$	2.2339(11)
Mn–N(2)	2.2565(13)	Mn–N(2)$^{\#1}$	2.2565(13)
O(1)–Mn–O(1)$^{\#1}$	97.12(7)	O(1)–Mn–N(2)$^{\#1}$	95.98(5)
O(1)–Mn–O(3)	88.06(4)	O(1)$^{\#1}$–Mn–N(2)$^{\#1}$	164.69(5)
O(1)$^{\#1}$–Mn–O(3)	92.24(4)	O(1)–Mn–N(2)	164.69(5)
O(1)–Mn–O(3)$^{\#1}$	92.24(4)	O(1)$^{\#1}$–Mn–N(2)	95.98(5)
O(1)$^{\#1}$–Mn–O(3)$^{\#1}$	88.06(4)	O(3)–Mn–N(2)	83.55(5)
O(3)–Mn–O(3)$^{\#1}$	179.55(7)	O(3)$^{\#1}$–Mn–N(2)	96.09(5)
O(3)–Mn–N(2)$^{\#1}$	96.09(5)	O(3)$^{\#1}$–Mn–N(2)$^{\#1}$	83.55(5)
N(2)$^{\#1}$–Mn–N(2)	72.32(6)		
4			
Mn–O(1)	2.1301(12)	Mn–O(3)$^{\#1}$	2.2602(14)
Mn–O(1)$^{\#1}$	2.1301(12)	Mn–O(3)	2.2602(14)
Mn–N(2)	2.2447(14)	Mn–N(2)$^{\#1}$	2.2447(14)
O(1)–Mn–O(1)$^{\#1}$	95.97(8)	O(1)–Mn–N(2)	164.12(5)
O(1)–Mn–O(3)	95.63(5)	O(1)–Mn–N(2)$^{\#1}$	96.17(6)
O(1)–Mn–O(3)$^{\#1}$	88.08(5)	O(1)$^{\#1}$–Mn–N(2)	96.17(6)
O(1)$^{\#1}$–Mn–O(3)$^{\#1}$	95.63(5)	O(1)$^{\#1}$–Mn–N(2)$^{\#1}$	164.12(5)
O(1)$^{\#1}$–Mn–O(3)	88.08(5)	N(2)–Mn–O(3)	94.97(5)
O(3)$^{\#1}$–Mn–O(3)	174.48(8)	N(2)–Mn–O(3)$^{\#1}$	80.58(5)
N(2)$^{\#1}$–Mn–O(3)	80.58(5)	N(2)$^{\#1}$–Mn–O(3)$^{\#1}$	94.97(6)
N(2)$^{\#1}$–Mn–N(2)	73.96(7)		

Symmetry transformations used to generate equivalent atoms: for **1**, $^{\#1}$ $-x+1$, y, $-z+1/2$; for **2**, $^{\#1}$ $x+1$, y, z; for **3**, $^{\#1}$ $-x+2$, y, $-z+3/2$; for **4**, $^{\#1}$ $-x$, y, $-z+3/2$.

Table 3
Hydrogen bonds for **1–4** (Å and deg)

1				
D–H···A	d(D–H)	d(H···A)	d(D···A)	<(DHA)
C(15)–H(15)···O(1)$^{\#3}$	0.91(3)	2.67(3)	3.484(4)	149(3)
2				
D–H···A	d(D–H)	d(H···A)	d(D···A)	<(DHA)
O(5)–H(5AA)···O(2)$^{\#3}$	0.81(3)	1.88(3)	2.679(2)	174(3)
O(5)–H(5BA)···O(3)$^{\#4}$	0.87(3)	1.92(3)	2.763(2)	163(3)
C(24)–H(24A)···O(2)$^{\#5}$	0.93	2.58	3.334(3)	138.4
C(27)–H(27A)···O(4)$^{\#6}$	0.93	2.50	3.154(3)	127.9
C(14)–H(14A)···O(3)	0.93	2.40	3.006(3)	122.3
3				
C(2)–H(2)···O(3)$^{\#3}$	0.972(17)	2.598(17)	3.478(2)	150.7(13)
C(14)–H(14)···O(2)$^{\#4}$	0.90(2)	2.58(2)	3.478(2)	172.8(18)
C(15)–H(15)···O(3)$^{\#4}$	0.984(18)	2.533(18)	3.336(2)	138.7(14)
C(8)–H(8)···O(2)$^{\#5}$	0.92(2)	2.600(18)	3.358(2)	140.2(16)
O(3)–H(3B)···N(1)$^{\#6}$	0.79(2)	2.19(2)	2.9780(17)	171(2)
O(3)–H(3A)···O(2)	0.90(2)	1.78(2)	2.6527(16)	165.1(19)
C(2)–H(2)···N(1)$^{\#2}$	0.972(17)	2.482(17)	2.822(2)	100.2(12)
4				
C(2)–H(2)···O(3)$^{\#3}$	0.978(19)	2.675(19)	3.562(2)	150.9(15)
C(2)–H(2)···N(1)$^{\#2}$	0.978(19)	2.449(19)	2.814(2)	101.6(13)
C(5)–H(5)···O(2)$^{\#4}$	0.85(2)	2.69(2)	3.451(2)	149.9(19)
C(11)–H(11)···O(3)$^{\#5}$	0.96(2)	2.62(2)	3.423(3)	140.5(17)
C(13)–H(13)···O(2)$^{\#6}$	0.94(2)	2.68(2)	3.278(2)	122.1(17)
O(3)–H(3W1)···N(1)$^{\#6}$	0.69(2)	2.40(2)	3.084(2)	171(3)
O3–H3W2···O2$^{\#1}$	0.882	1.773	2.636	165.67
O3–H3W2···O1$^{\#1}$	0.882	2.622	3.053	111.19

Symmetry transformations used to generate equivalent atoms: for **1**: $^{\#1}$ $-x+1$, y, $-z+1/2$; $^{\#2}$ $-x+1$, $-y$,$-z$, $^{\#3}$ x, $y+1$, z; for **2**: $^{\#1}$ $x+1$, y, z; $^{\#2}$ $x-1$, y, z; $^{\#3}$ $-x+1$, $-y$, $-z+1$; $^{\#4}$ $-x$, $-y$, $-z+1$; $^{\#5}$ $x+1/2$, $-y-1/2$, $z+1/2$; $^{\#6}$ $-x+1/2$, $y-1/2$, $-z+3/2$; for **3**: $^{\#1}$ $-x+2$, y, $-z+3/2$; $^{\#2}$ $-x+3/2$, $-y+3/2$, $-z+2$; $^{\#3}$ x, $-y+1$, $z+1/2$; $^{\#4}$ $-x+2$, $-y+1$,$-z+1$; $^{\#5}$ $-x+3/2$, $y+1/2$, $-z+3/2$; $^{\#6}$ $-x+3/2$, $y-1/2$, $-z+3/2$; for **4**: $^{\#1}$ $-x$, y, $-z+3/2$; $^{\#2}$ $-x+1/2$, $-y+1/2$, $-z+1$; $^{\#3}$ $-x$, $-y+1$, $-z+1$; $^{\#4}$ $-x+1/2$, $y-1/2$, $-z+3/2$; $^{\#5}$ x, $-y+1$, $z+1/2$; $^{\#6}$ $x-1/2$, $y+1/2$, z.

weight of 14.03% is zinc oxide that is in agreement with the calculated value of 13.84% (Fig. 1a). The TGA result indicates that **2** begin to decompose at 218 °C and display three stages of weight loss. The first weight loss of 3.01% from 218 to 280 °C is due to the loss of water molecules, which is exactly corresponding to the release of coordinated water molecules (calculated value 3.09%). Upon increasing temperature two-step total weight loss between 318 and 603 °C is consistent with the loss of bqdc and bpy ligands. The remaining weight of 14.08% is zinc oxide that is in agreement with the calculated value of 13.99% (Fig. 1b). The TGA result indicates that **3** begins to decompose at 130 °C and the first weights loss of 6.19% from 130 to 269 °C are attributed to the loss of water molecules (calculated value 6.11%), which was followed by a two-step total weight loss of bqdc and bpy ligands (Fig. 1c). **4** exhibits similar TGA characteristic to **3** (Fig. 1d). The TGA studies of compounds **1–4** demonstrate that **1** is more stable compared with **2–4**. This is due to that carboxylate-oxygen atoms adopt bidentate chelating coordination mode (Scheme 1a) with metal atoms, moreover, there is not coordination water molecule exists in **1**.

In addition, the chemistry and humidity stabilities of **1–4** are quite good due to that they were synthesized under hydrothermal condition. Aqueous solution and common organic solvents cannot lead to the decomposition of **1–4**. They also display photo-stability and do not destruct under UV light. However, **1–4** are unstable in strong acid aqueous solution such as H_2SO_4 and HCl.

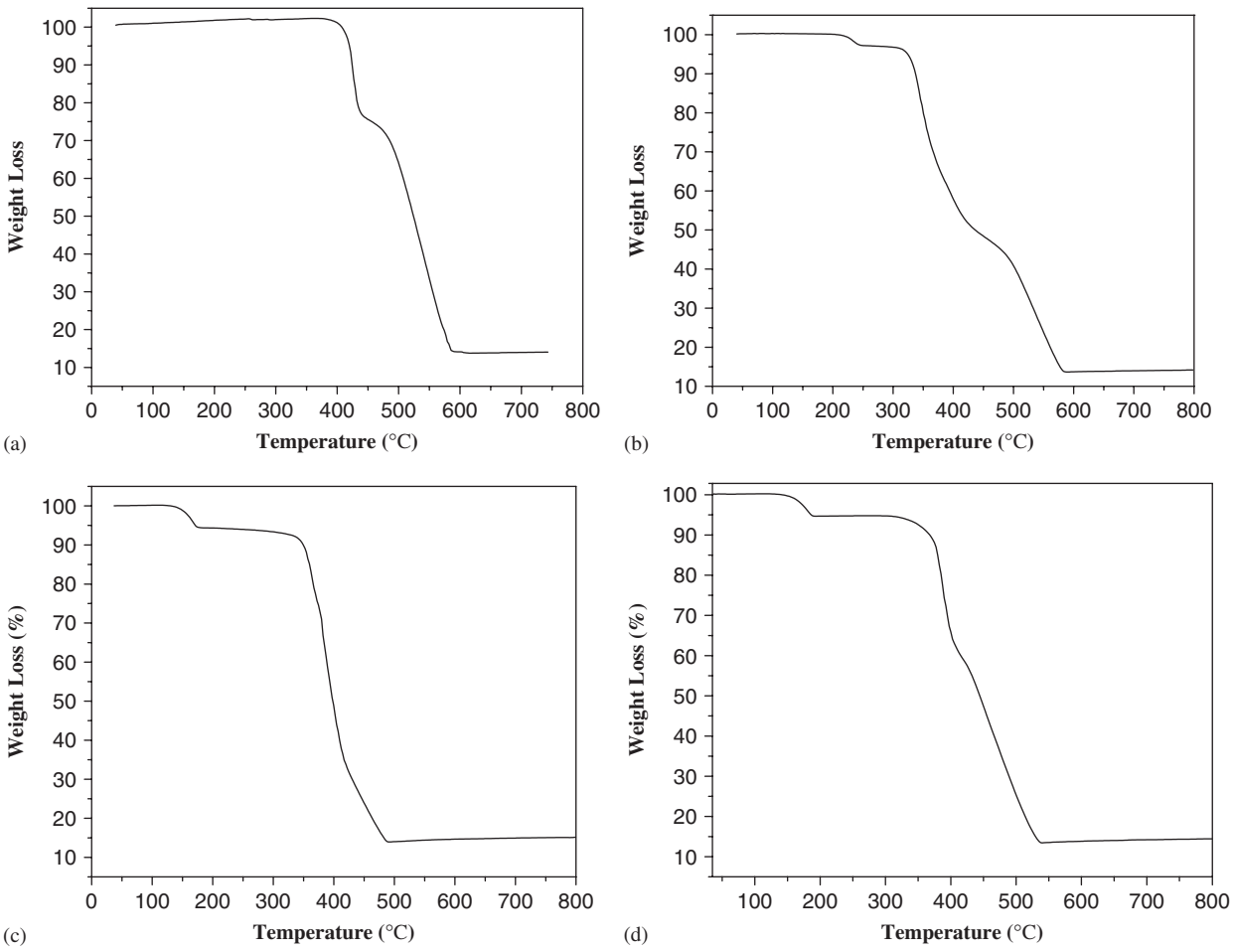

Fig. 1. The TGA diagram for the coordination polymers: (a) **1**; (b) **2**; (c) **3**; (d) **4**.

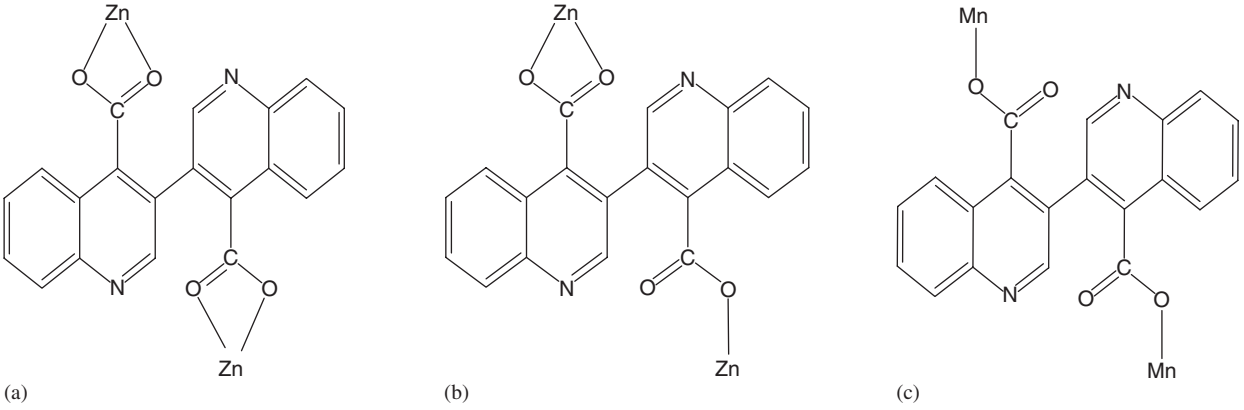

Scheme 1. The coordination modes of the carboxylate group: (a) bis-bidentate chelating; (b) monodentate and bidentate chelating; (c) bis-monodentate.

3.3. Description of structures

3.3.1. $[Zn(bqdc)(phen)]_n$ 1 and $[Zn(bqdc)(bpy)(H_2O)]_n$ 2

In the crystal structure of **1**, the coordination environment around the Zn atom can be described as highly distorted octahedral with two nitrogen atoms (Zn–N2 = 2.097(2) Å, and Zn–N2A = 2.097(2) Å) from a chelating phen ligand, four carboxylate-oxygen atoms (Zn–O1 = 2.2255(2) Å, Zn–O1A = 2.2255(2) Å, Zn–O2 = 2.1027(2) Å, and Zn–O2A = 2.1027(2) Å) from two bqdc ligands (Fig. 2). Two nitrogen atoms N2, N2A and two carboxylate-oxygen atoms O1, O1A comprise the equatorial plane, while the other two carboxylate-oxygen atoms O2, O2A occupy the axial positions. The axial Zn–O distances are slightly shorter than the equatorial Zn–O distances.

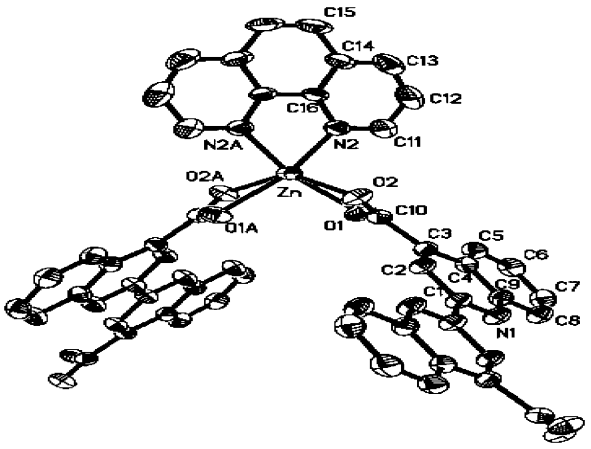

Fig. 2. Perspective view of the coordination environment of the zinc atom in **1** and including the asymmetric unit is represented by thermal ellipsoids drawn to encompass 50% of their electron density.

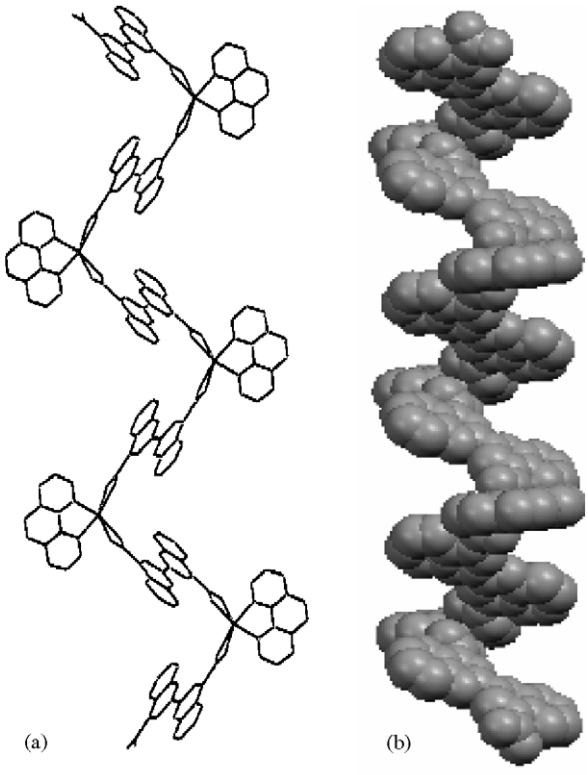

Fig. 3. Side view (a) and space-filling view (b) of the single helix-like chain in **1**.

In **1**, each bqdc ligand adopts a μ_2-bridging mode to connect with two zinc atoms and the O-donors adopt bidentate chelating coordination mode (Scheme 1a). Thus, each bqdc ligand links two zinc centers and each zinc center connects with two bqdc ligands to form the single helix-like chain structure (Fig. 3). In each chain, two adjacent Zn atoms are bridged by a bqdc ligand with Zn⋯Zn distance of 12.992 Å. The phen ligands are alternately attached to both sides of a chain and parallel to each other. Each phen ligand acts as a chelating ligand with a typical Zn–N distance 2.097(2) Å and N–Zn–N angles 79.46(1)°. To our knowledge, up to now only two examples containing bqdc ligand have been reported, in which each bqdc ligand binds two metal ions in a bis-monodentate mode [27,28].

The hydrogen bonding and $\pi\cdots\pi$ stacking interactions often play important roles in controlling molecular conformation, molecular aggregation, and the function of a vast number of chemical systems ranging from inorganic to biological [29–31]. These interactions not only have been widely used to construct extended organic supramolecular structures, but also been employed to construct MOFs. They can cause critically influence on structure, metal coordination geometry and stability of MOFs [32–34]. The C–H⋯O hydrogen bond interactions in **1** are found between adjacent chains (Fig. 4). The hydrogen bond distance and angle are 3.484 Å for C15⋯O1 and 149.3° for C15–H15⋯O1, respectively. These C–H⋯O hydrogen bonds form a double-linked C–H⋯O hydrogen bonding interactions resulting in the formation of the layers. A similar example of the hydrogen bonded layer [Zn(bpy)(tp)](bpy) was reported recently [35].

In the crystal structure of **2** (Fig. 5a), the coordination environment of zinc atom can be described as distorted octahedral with two nitrogen atoms [Zn–N3 2.1044(2) Å and Zn–N4 2.1651(2) Å] from a bpy ligand, three carboxylate-oxygen atoms [Zn–O1 1.9735(2) Å, Zn–O3A 2.3870(2) Å, and Zn–O4A 2.1103(2) Å] from two different bqdc ligands and one oxygen atom [Zn–O5 2.1068(2) Å] from a water molecular. Each bqdc ligand links two Zn atoms and each zinc atom connects with two bqdc ligands to form the chain structure. In each chain two adjacent Zn atoms are bridged by a bqdc ligand with Zn⋯Zn distance of 13.656 Å (Fig. 5b).

It is worth noting that there are distinct differences between the structures of **1** and **2**, although both of them exhibit one-dimensional chain topology. For **1**, two carboxylate groups of each bqdc ligand coordinated with two metal atoms by bidentate chelating fashion to form helix-like chain. While for **2**, two carboxylate groups of a bqdc ligand exhibit different coordination modes, namely one carboxylate group coordinated with a Zn atom by bidentate chelating mode and the other one by monodentate mode (Scheme 1b). The Zn atoms exhibit nearly linear arrangement within each chain with Zn⋯Zn⋯Zn angles 180.00°. Compound **1** displays a layered structure feature based on hydrogen bonding interactions. In **2**, all coordination chains array along *a*-axis and are linked together via hydrogen bonding and $\pi\cdots\pi$ stacking interactions resulting in a three-dimensional structure (Fig. 6).

There are two types of hydrogen bonds between adjacent chains in **2**. One type of hydrogen bond involves the coordinated oxygen atoms of water molecules and uncoordinated carboxylate oxygen atoms with the O5⋯O2 distance of 2.679 Å and O5–H5⋯O2 angle of 174.3°, the

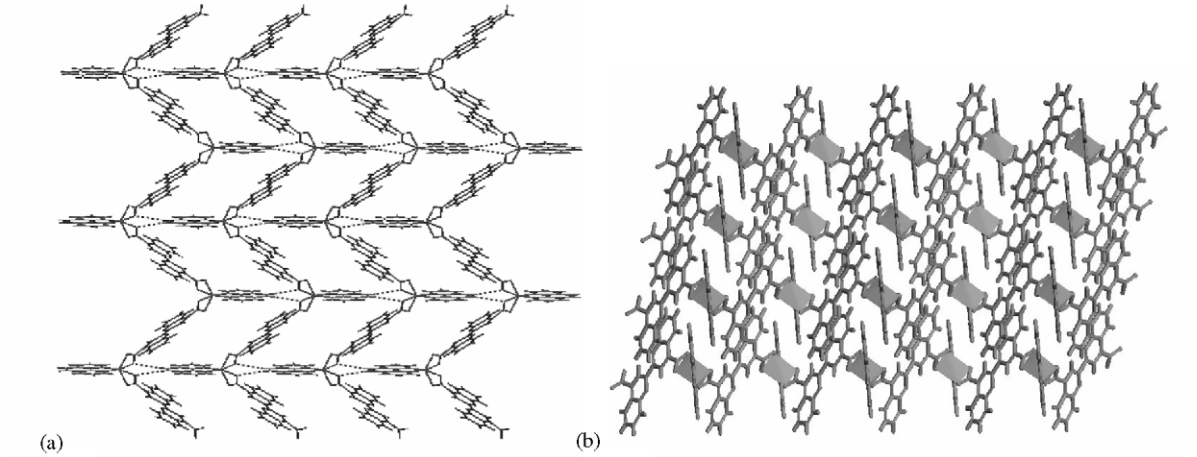

Fig. 4. The hydrogen-bonding between chains (a) and perspective view of the structure along the *b*-axis (b) in **1**.

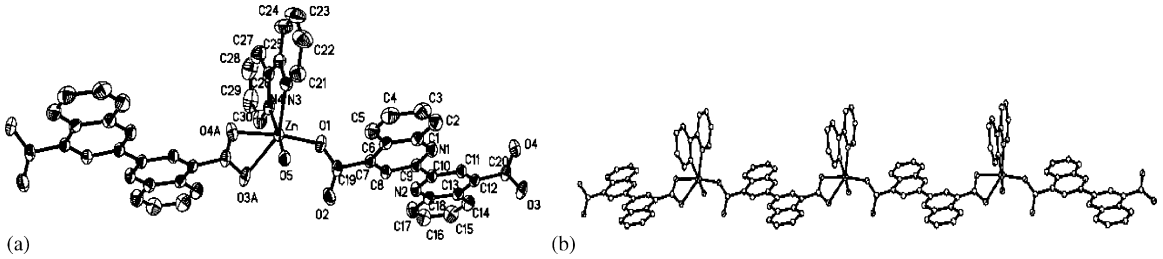

Fig. 5. Coordination environment around zinc atom with the thermal ellipsoids at 50% probability level (a) and single chain (b) in **2**.

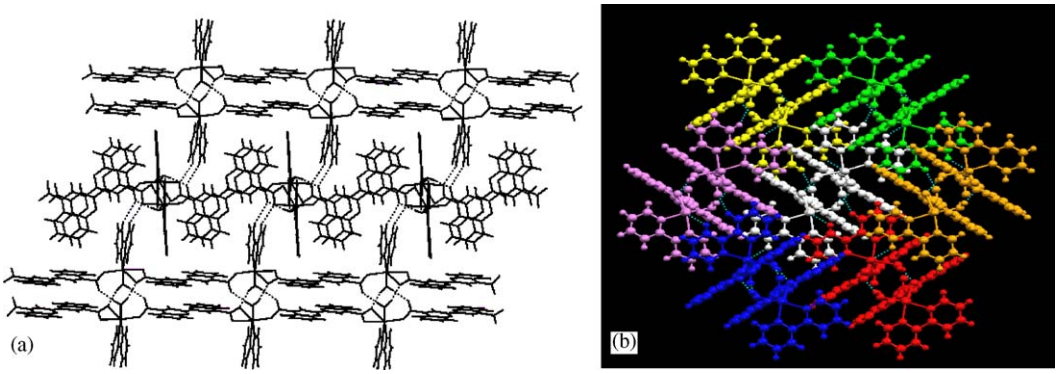

Fig. 6. (a) Perspective view of the hydrogen-bond and $\pi\cdots\pi$ stacking interactions between chains and chain-dimers in **2**. (b) The packing of **2** viewed down the *a*-axis.

other type of hydrogen bond involves the coordinated oxygen atoms of water molecules and coordinated carboxylate oxygen atoms with the O5⋯O3 distance of 2.763 Å and O5–H5⋯O3 angle of 163.3°. These two kinds of hydrogen bonding interactions lead to the formation of chain-dimers (Fig. 6a). Additionally, there are strong $\pi\cdots\pi$ stacking interactions with contact distance of 3.556 Å between the aromatic rings of the bqdc ligands within a chain-dimer. The chain-dimers are linked together by two kinds of C–H⋯O hydrogen bonding interactions with the C24⋯O2 distance of 3.334 Å and the C27⋯O4 distance of 3.154 Å (Fig. 6b). For two adjacent chain-dimers, weak $\pi\cdots\pi$ stacking interactions exist between bpy ligands and the contact distance is 3.831 Å and each chain-dimer is surrounded by six chain-dimers.

3.3.2. [Mn(bqdc)(bpy)(H$_2$O)$_2$]$_n$ 3 and [Mn(bqdc)(phen)(H$_2$O)$_2$]$_n$ 4

In the crystal of **3**, the independent unit consists of one Mn atom, one bqdc ligand, one chelating bpy ligand and two coordinated water molecules. Each Mn atom is six coordinated by two nitrogen atoms of one bpy ligand, two carboxylate-oxygen atoms of two bqdc ligands and two oxygen atoms of two water molecules (Fig. 7a). The Mn–O

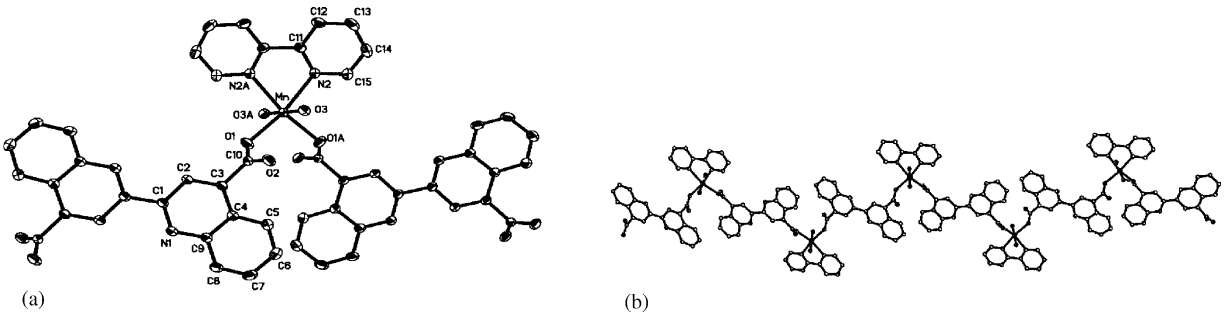

Fig. 7. Coordination environment around manganese atom with the thermal ellipsoids at 50% probability level (a) and single chain (b) in **3**.

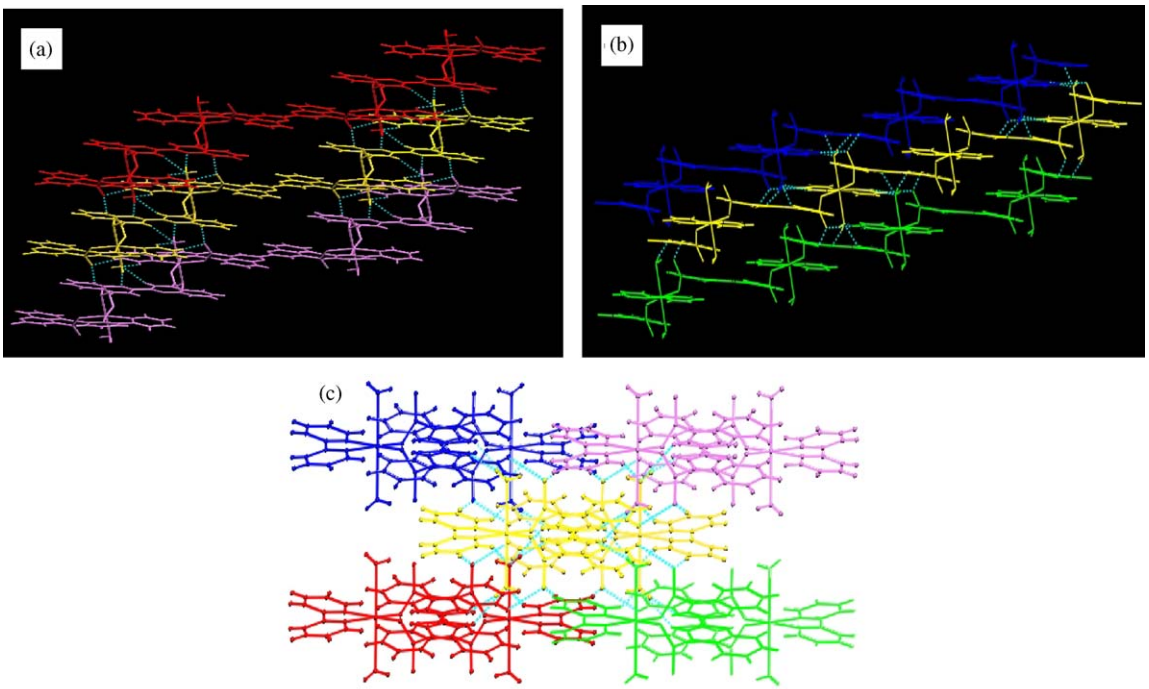

Fig. 8. Perspective view of the hydrogen-bond between chains in **3**.

bond distances are in the range from 2.1494(1) to 2.2339(1) Å, and the average Mn–N distance is 2.2565(1) Å. Two nitrogen atoms (N2 and N2A) and two carboxylate-oxygen atoms (O1 and O1A) comprise the equatorial plane; the other two water molecule atoms occupy the axial positions. The bond distance of Mn–O3 (2.2339(1) Å) in the axial position is slightly longer than that of Mn–O1 (2.1494(1) Å) in the equatorial plane.

The two carboxylate groups of the bqdc ligand in **3** display a syn-anti bis-monodentate bridging coordination mode, shown in Scheme 1c. Each bqdc ligand adopts μ_2-bridging mode coordinating to two Mn atoms resulting in the formation of one-dimensional zig-zag chains (Fig. 7b). The Mn···Mn···Mn angle within a chain is 112.55°, the distance between the two Mn atoms that are bridged by a bqdc ligand is 13.969 Å. Within a zig-zag chain, the free carboxyl oxygen atom O2 forms an intermolecular hydrogen bond with the coordinated oxygen of the water molecule (O3···O2 2.6527(2) Å, O3–H3A···O2 165.1(2)°). Moreover, the coordinated water molecule as hydrogen bond donor forms hydrogen bond with nitrogen of bqdc ligand (O3···N1 2.9780(2) Å; O3–H3B···N1 171(2)°). Obviously, two nitrogen atoms of a bqdc ligand contact with the two water molecules on the other two different chains, respectively. There are also involved four hydrogen bonds via C–H···O interactions (C2···O3 3.478(2) Å and C2–H2···O3 150.7(1)°; C15···O3 3.336(2) Å and C15–H15 ···O3 138.7(1)°; C8···O2 3.358(2) Å and C8–H8···O2 140.2(2)°; C14···O2 3.478(2) Å and C14-H14···O2 172.8(2)°) between two adjacent chains. As a result, each chain connects with four nearest-neighboring chains by hydrogen bonding interactions resulting in the formation of extended three-dimensional networks (Fig. 8). For two adjacent chains, weak $\pi\cdots\pi$ stacking interactions exist between bpy and bqdc ligands and the contact distance is 3.467 Å (Fig. 9).

In the crystal of **4**, the asymmetric unit contains 0.5 Mn atom, 0.5 bqdc ligands, 0.5 chelating phen ligands and one water molecule. The Mn atom is six-coordinated by two nitrogen atoms of one phen ligand, four oxygen atoms of two different bqdc ligands and two different water molecules (Fig. 10a). The Mn–O bond distances are in the range from 2.1301(1) to 2.2602(1) Å. Each bqdc ligand displays syn-anti bis-monodentate bridging coordination mode with two Mn centers resulting in the formation of the zig-zag chain structure (Fig. 10b). The observed Mn···Mn···Mn angle within a chain is 109.78°. The supramolecular structure of **4** is very similar to **3** and exhibits three-dimensional architecture via hydrogen bonding (Fig. 11).

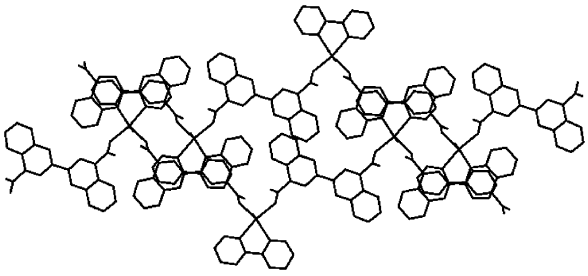

Fig. 9. Perspective view of the $\pi\cdots\pi$ stacking interactions between chains in **3**.

3.4. Emission and magnetic properties

The diffuse reflectance UV-visible spectra (Fig. 12) of the **1**–**4** in solid state exhibit two absorption bands at around 240 and 330 nm, which are due to the $\pi \rightarrow \pi^*$ electronic transitions of bqdc and phen (or bpy) ligands. The photoluminescent (PL) spectra of **1, 2**, phen, bqdc and $(phen)_2ZnCl_2$ are presented in Fig. 13. The emission peaks of **1** and **2** are 387 and 426 nm, respectively. By comparing the emission spectra of **1**, phen, bqdc and $(phen)_2ZnCl_2$ we can conclude that the emission spectrum of **1** includes both of phen and bqdc emission properties. This means that both of phen and bqdc contribute to the emission of **1**. 1,10-phenathroline-based chromophores often exhibited emission red-shift upon coordination with Zn^{2+} ions, which was attributed to that Zn^{2+} ions could resulted in the changes of HOMO and LUMO energy levels of 1,10-phenathroline [36,37]. Compound **2** exhibits similar emission property to H_2bqdc ligand suggesting that the emission of **2** originated from the $\pi \rightarrow \pi^*$ electronic transition excited state of bqdc. The emission spectrum of **2** only shows the emission property of bqdc ligand because bpy does not exhibit emission. The other possible explanation for the difference emission properties of **1** and **2** is that the different coordination modes of bqdc ligands in **1** and **2** may result in the difference of emission. Because the stability of **1** is very good, it is possible to develop high

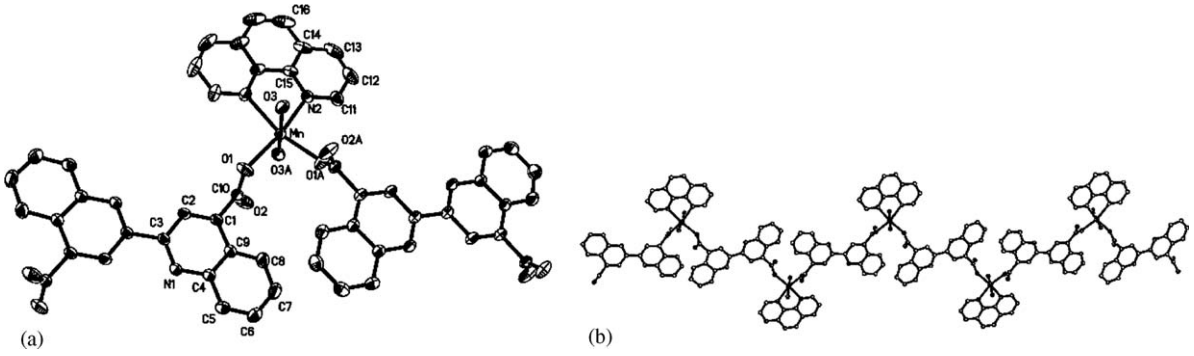

Fig. 10. Coordination environment around manganese atom with the thermal ellipsoids at 50% probability level (a) and single chain (b) in **4**.

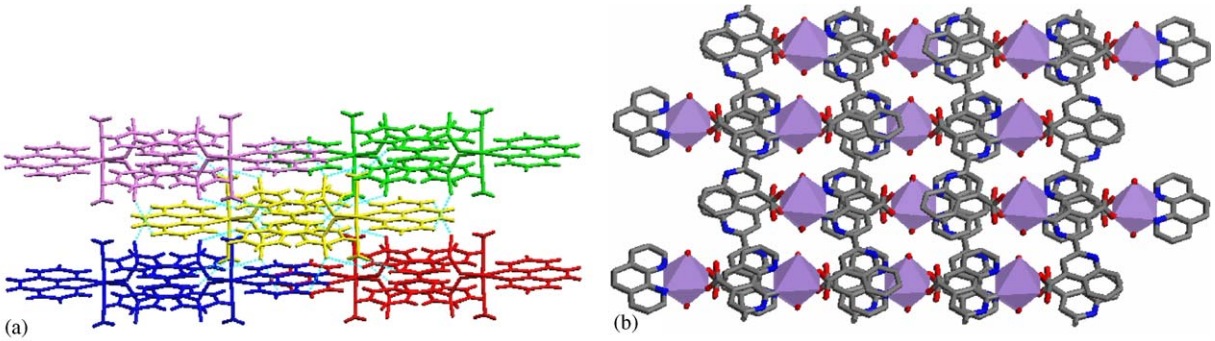

Fig. 11. Perspective view of the hydrogen-bonding between chains (a) and the packing viewed down the *a*-axis (b) in **4**.

stable luminescent materials based on **1**. The emission intensities are not quite strong and the PL quantum yields of **1** and **2** should be not very high. At present time, we cannot measure the solid-state PL quantum yields of **1** and **2** due to the limitation of our fluorescent spectrometer. It is well known that the luminescent property of molecule-based materials depend directly on the arrangement and relative orientation of the constituent molecules. Therefore, fine-tuning of the performance of luminescent materials need to drive the molecular self-assembly toward highly ordered, reproducible, and stable supramolecular structures in solid state. For conventional molecule based luminescent materials, it is very difficult to control the molecular arrangement in solid state. But crystal engineering is providing a new way to make predictably ordered luminescent coordination polymer materials such as optically anisotropic and stable materials. On the other hand, the rigidity of coordination polymers is stronger compared with conventional molecule materials, which can reduce the loss of energy via vibration motions and increasing the emission efficiency [38].

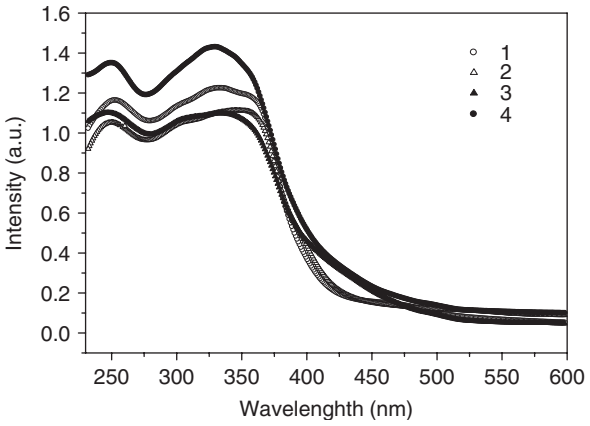

Fig. 12. Diffuse reflectance UV-visible spectra of **1**–**4**.

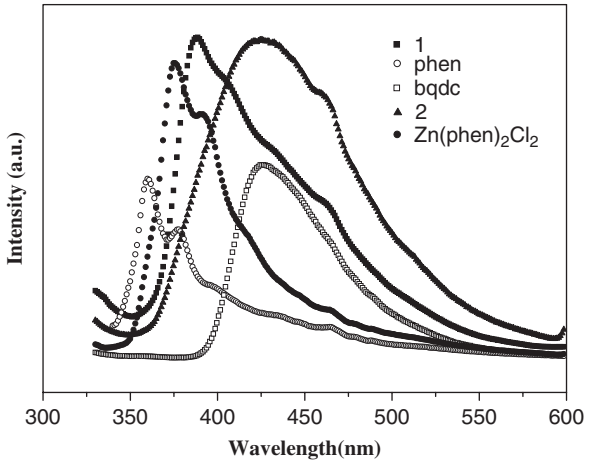

Fig. 13. Solid-state emission spectra of phen, H_2bqdc, $(phen)_2ZnCl_2$, **1** and **2** at room temperature.

The temperature-dependent magnetic properties of **3** and **4** were studied. The susceptibility curve of χ_m and $\chi_m T$ versus T in the full temperature range for **3** and **4** are presented in Fig. 14. The effective magnetic moment per metal atom of **3** and **4** is 5.46 and 5.50 μ_B at 300 k, respectively. For **3**, the $\chi_m T$ value is 3.73 $cm^3\,K\,mol^{-1}$ at 300 K, which gradually increased upon decreasing temperature ($\chi_m T = 4.70\,cm^3\,K\,mol^{-1}$ at 10 K). This phenomenon suggests that the presence of ferromagnetic exchange interactions between Mn centers in this system. The $\chi_m T$ value decreases quickly when the temperature is below 10 K and reach 4.54 $cm^3\,K\,mol^{-1}$ at 2 K demonstrating that there are antiferromagnetic coupled interactions in this temperature range for **3**. The plot of χ_m^{-1} versus T over the temperature accords with the Curie–Weiss law $\chi_m = c_m/(T-\Theta)$. The $\chi_m T - T$ characteristic of **4** shows a value of 3.78 $cm^3\,K\,mol^{-1}$ at 300 K. The $\chi_m T$ value continuously increases upon decreasing temperature and reaches a value of 4.48 $cm^3\,K\,mol^{-1}$ at 7 K. This indicates that ferromagnetic interactions exist in **4**. However, the $\chi_m T$ value drops quickly when the temperature is below 7 K and reaches 4.22 $cm^3\,K\,mol^{-1}$at 2 K indicating there is antiferromagnetic coupled interaction in compound in this temperature range. Compounds **3** and **4** exhibit similar temperature dependent magnetic properties. According to

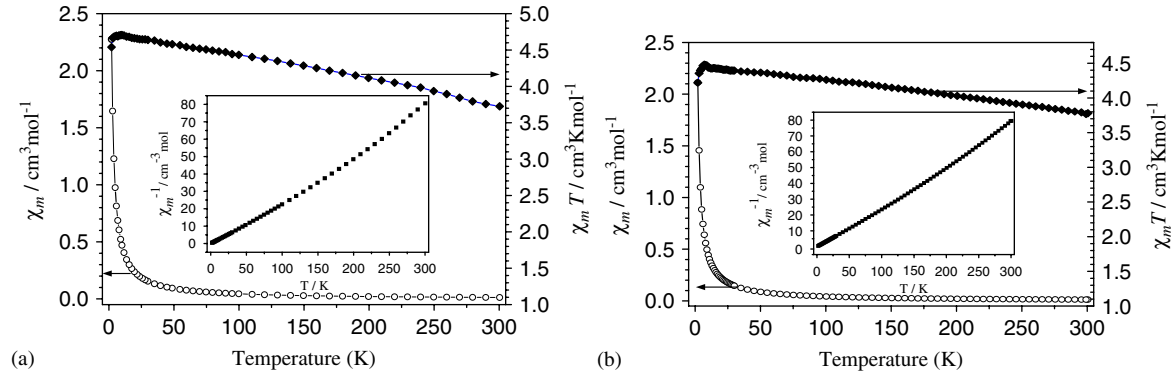

Fig. 14. Temperature variation of the magnetic susceptibility χ_m and $\chi_m T$ for **3** (a) and **4** (b), and χ_m^{-1}versus T (inset); the solid line represents the theoretical curve with the best fit parameters.

the crystal structures of **3** and **4**, the magnetic behaviors of **3** and **4** may be attributed to the existence of Mn–O–C–O–Mn connectivity and Mn···Mn superexchange interaction. The magnetic behaviors of compounds **3** and **4** are similar to those of related Ni, Cu, Mn compounds [39–41]. To learn how to design and synthesize materials with expected magnetic property is one of challenge requires in modern material science. Meeting this challenge requires rational selection of individual molecular components and ingenious control of the arrangement and interaction of neighboring molecules. The coordination polymers with well-defined supramolecular architectures provide an opportunity to realize above ideal.

4. Conclusions

Four new coordination polymers based on H_2bqdc, phen and bpy have been synthesized and characterized by single crystal X-ray diffractions. In **1–4**, one-dimensional coordination molecular chains exist and specially, single helix-like chains were found in **1**. For **1**, the one-dimensional coordination chains are linked together by hydrogen bonding resulting in the formation of layered structure characteristic and for **2–4** hydrogen bonding and (or) $\pi\cdots\pi$ stacking interactions lead to the formation of three-dimensional architectures. TGA studies demonstrate that **1** is a stable coordination polymer. Compounds **1** and **2** display novel emission properties. The progress that ferromagnetic exchange interactions change into antiferromagnetic coupled interactions exists in **3** and **4** system upon decreasing temperature. The synthesis, single crystal studies and spectroscopic characterizations of coordination polymers **1–4** enrich the coordination polymer systems based on polycarboxylates and transition metals. We have demonstrated that the one-, three-dimensional coordination polymers based on bqdc, which contain other metals such as Cu^{2+}, La^{3+} and Sm^{3+} could be synthesized under hydrothermal conditions. Their synthesis, structures and properties will be reported in other papers. Hydrothermal method is an efficient route for the synthesis coordination polymers based on bqdc ligand.

Supporting information available

X-ray crystallographic files in CIF format deposited with the Cambridge Structural Database as files CCDC-271609, -271610, -271612, and -271611, respectively, for crystal 1–4. These data can be obtained free of charge via www.ccdc.cam.ac.uk/conts/retrieving.html [or from the Cambridge Crystallographic Data Center, 12 Union Road, Cambridge CB2 1EZ, UK; Fax: (internat.) +44 1223 336 033; E-mail: deposit@ccdc.cam.ac.uk].

Acknowledgments

This work was supported by the National Natural Science Foundation of China (50225313, 50520130316 and 50573030), the Major State Basic Research Development Program (2002CB613401) and Program for Changjiang Scholars and Innovative Research Team in University (IRT0422).

Appendix A. Supplementary Data

Supplementary data associated with this article can be found in the online version at doi:10.1016/j.jssc.2005.11.003.

References

[1] K. Uemura, S. Kitagawa, K. Fukui, K. Saito, J. Am. Chem. Soc. 126 (2004) 3817.
[2] C.N.R. Rao, S. Natarajan, R. Vaidhyanathan, Angew. Chem. Int. Ed. 43 (2004) 1466.
[3] O.M. Yaghi, H. Li, C. Davis, D. Richardson, T.L. Groy, Acc. Chem. Res. 31 (1998) 474.
[4] B. Moulton, M.J. Zaworotko, Chem. Rev. 101 (2001) 1629.
[5] H. Li, M. Eddaoudi, M. O'Keeffe, O.M. Yaghi, Nature 402 (1999) 276.
[6] X.J. Li, R. Cao, Y.Q. Sun, W.H. Bi, X. Li, Y.Q. Wang, Eur. J. Inorg. Chem. 2 (2005) 321.
[7] P.J. Hagrman, D. Hagrman, J. Zubieta, Angew. Chem. Int. Ed. 38 (1999) 2638.
[8] S.S.Y. Chui, S.M.F. Lo, J.P.H. Charmant, G. Orpen, I.D. Williams, Science 283 (1999) 1148.
[9] J.S. Seo, D. Whang, H. Lee, S.I. Jun, J. Oh, Y.J. Jeon, K. Kim, Nature 404 (2000) 982.
[10] A.J. Blake, N.K. Champness, P. Hubbersley, W.S. Li, M.A. Withersly, M. Schöder, Coord. Chem. Rev. 183 (1999) 117.
[11] L. Chen, M. Eddaoudi, S.T. Hyde, M. O'Keeffe, O.M. Yaghi, Science 291 (2001) 1021.
[12] K. Barthelet, J. Marrot, D. Riou, G. Ferey, Angew. Chem. Int. Ed. 41 (2002) 281.
[13] M. Fujita, Y.J. Kwon, S. Washizu, K. Ogura, J. Am. Chem. Soc. 116 (1994) 1151.
[14] C. Janiak, Temizdemir, S. Scharmann, T.G. Schmalstieg, J. Demtschuk, Z. Anorg. Allg. Chem. 626 (2000) 2053.
[15] O.M. Yaghi, H. Li, C. Davis, D. Richardson, T.L. Groy, Acc. Chem. Res. 31 (1998) 474.
[16] J. Tao, M.L. Tong, X.M. Chen, J. Chem. Soc. Dalton Trans. 20 (2000) 3669.
[17] H. Gudbjartson, K. Biradha, K.M. Poirier, M.J. Zaworotko, J. Am. Chem. Soc. 121 (1999) 2599.
[18] S.M. Humphrey, R.A. Mole, J.M. Rawson, P.T. Wood, J. Chem. Soc. Dalton Trans. 11 (2004) 1670.
[19] J.M. Li, H.Q. Zeng, J.H. Chen, Q.M. Wang, X.T. Wu, Chem. Commun. 13 (1997) 1213.
[20] L.J. Zhang, J.Q. Xu, Z. Shi, X.L. Zhao, T.G. Wang, J. Solid State Chem. 32 (2003) 32.
[21] D.F. Sun, R. Cao, Y.C. Liang, Q. Shi, W.P. Su, M.C. Hong, J. Chem. Soc. Dalton Trans. 16 (2001) 2335.
[22] M.L. Tong, B.H. Ye, J.W. Cai, X.M. Chen, S.W. Ng, Inorg. Chem. 37 (1998) 2645.
[23] L.J. Zhang, J.Q. Xu, Z. Shi, W. Xu, T.G. Wang, J. Chem. Soc. Dalton Trans. 8 (2003) 1148.
[24] M. Petrov, Russ. Phys. Chem. (2003) 214.
[25] M. Makowska-Janusik, E. Gondek, I.V. Kityk, J. Wisla, J. Sanetra, A. Danel, Chem. Phys. 306 (2004) 265.
[26] G.M. Sheldrick, SHELXS-97, Program for Crystal Structure Solution, University of Göttingen, Göttingen, 1997.
[27] K.S. Min, M.P. Suh, Eur. J. Inorg. Chem. 2 (2001) 449.
[28] Y. Wang, R. Cao, W.H. Bi, X. Li, X.J. Li, D.F. Sun, J. Mol. Struct. 738 (2005) 51.

[29] T. Steiner, Angew. Chem. Int. Ed. 41 (2002) 48.
[30] A. Dkhissi, L. Adamowicz, G. Maes, Chem. Phys. Lett. 324 (2000) 127.
[31] A.J.A. Aquino, D. Tunega, G. Haberhauer, M.H. Gerzabeck, H. Lischka, J. Phys. Chem. A 106 (2002) 1862.
[32] V.A. Russell, M.C. Etter, M.D. Ward, J. Am. Chem. Soc. 116 (1994) 1941.
[33] F. Garcia-Tellado, S.J. Geib, S. Goswami, A.D. Hamilton, J. Am. Chem. Soc. 113 (1991) 9265.
[34] G.R. Desiraju, Acc. Chem. Res. 29 (1996) 441.
[35] X.M. Zhang, M.L. Tong, M.L. Gong, X.M. Chen, Eur. J. Inorg. Chem. 1 (2003) 138.
[36] H.S. Joshi, R. Jamshidi, Y. Tor, Angew. Chem. Int. Ed. 38 (1999) 2722.
[37] J.C. Loren, J.S. Siegel, Angew. Chem. Int. Ed. 40 (2001) 754.
[38] H. Yersin, A. Vogler (Eds.), Photochemistry and Photophysics of Coordination Compounds, Springer, Berlin, 1987.
[39] Y.G. Li, N. Hao, Y. Lu, E.B. Wang, Z.H. Kang, C.W. Hu, Inorg. Chem. 42 (2003) 3119.
[40] E.Q. Gao, S.Q. Bai, C.F. Wang, Y.F. Yue, C.H. Yan, Inorg. Chem. 42 (2003) 8456.
[41] P. Cheng, S.P. Yan, C.Z. Xie, B. Zhao, X.Y. Chen, X.W. Liu, C.H. Li, D.Z. Liao, Z.H. Jiang, G.L. Wang, Eur. J. Inorg. Chem. (2004) 2369.